Nuclear Science and Techniques (2025) 36:191
https://doi.org/10.1007/s41365-025-01766-5

Nuclear deformation effects on α-decay half-lives with empirical formula and machine learning

Hong-Qiang You[1,2] · Xiao-Tao He[1] · Ren-Hang Wu[1] · Shuang-Shuang Zhang[1] · Jing-Jing Li[1] · Qing-Hua He[1] · Hai-Qian Zhang[1]

Received: 9 December 2024 / Revised: 20 January 2025 / Accepted: 2 February 2025 / Published online: 24 July 2025

Abstract
An improved formula considering the deformation effect for the α-decay half-lives is proposed based on WKB barrier penetrability. Using the quadrupole deformation values of the daughter nuclei obtained from the WS4 and FRDM models in the improved formula, the root mean square deviation (RMSD) between the calculated results and experimental data decreased from 0.456 to 0.413 and 0.415, respectively. Although the improved formula did not significantly reduce the overall RMSD, it produced results that better matched the experimental values for nuclei with larger deformations. Additionally, eXtreme Gradient Boosting (XGBoost) models were employed to further reduce the deviations between the calculated α-decay half-lives and experimental data, with the corresponding RMSDs decreasing from 0.413 to 0.295 and from 0.415 to 0.302, respectively. Furthermore, the improved empirical formula and XGBoost models were used to predict the α-decay half-lives of nuclei with $Z = 117$, 118, 119, and 120. The results suggest that $N = 184$ is the magic number.

Keywords α-decay · Nuclear deformation effects · Magic numbers · Superheavy nuclei

1 Introduction

In 1928, α-decay was first described as a quantum mechanical tunneling effect by Gurney and Condon [1] and Gamow [2]. Within Gamow's picture, the α cluster is preformed in the parent nucleus before it travels through a potential barrier. α-decay has been used as an important tool for understanding nuclear structure. Experimentally, because α-decay is the dominant decay mode of superheavy nuclei, detecting α-decay chains of synthesized superheavy nuclei (SHN) is an important method for identifying them. Consequently, α-decay remains a prominent and active area of study in nuclear physics [3–5].

Many empirical formulas have been proposed to study α -decay half-live. The earliest law for α-decay half-lives was formulated by Geiger and Nuttall [6], which states that the logarithm of α-decay half-lives $\log_{10}T_{1/2}$ is linearly correlated with the reciprocal of the square of α-decay energy Q_α. Subsequently, many additional empirical formulas have been introduced. Royer developed an analytical formula for α-decay under the framework of the generalized liquid drop model (GLDM) [7, 8]. According to the Viola and Seaborg (VSS) formula, certain parameters are used to describe α -decay half-lives by considering the unpaired nucleon blocking effect [9]. A unified description (UD) formula for the half-life and decay energy of complex cluster radioactivity was presented by Ni et al. [10]. Ren et al. improved the Geiger–Nuttall (G–N) law for α-decay half-lives by incorporating a parameter representing the shell effect in 2012 [11]. Qi proposed a universal decay law (UDL) using the structure of the R-matrix and microscopic mechanism of charged particle emission [12]. Additionally, improved formulas were proposed by adding asymmetry terms or angular momentum effects in Refs. [13, 14, 14–22].

This work was supported by the Joint Funds for the Innovation of Science and Technology, Fujian province (Nos. 2021Y9190 and 2021Y9210), National Natural Science Foundation of China (No. 12475121), and National Key R&D Program of China (Nos. 2023YFA1606503 and 2024YFE0109804).

✉ Xiao-Tao He
hext@nuaa.edu.cn

[1] Nanjing University of Aeronautics and Astronautics, Nanjing 210016, China

[2] Clinical Oncology School of Fujian Medical University, Fujian Cancer Hospital, Fuzhou 350014, China

In Refs. [23–30], the authors demonstrated that the deformation of nuclei plays an essential role in α-decay. The total energy, fission barrier, and Coulomb interaction of nuclei have been recalculated by incorporating deformation effects. The penetration probability of α particles is affected by the deformation effects [31]. The deformation and orientation of the daughter nucleus can change the slope and intercept of the linear relationship between $\log_{10}T_{1/2}$ and $Q^{-1/2}$ [32]. For SHN, the effects of nuclear deformation on α-decay half-lives were explored [33]. Studies investigating the impact of deformation effects on α-decay half-lives have been conducted based on macro-micro and microscopic models. The results indicate that considering deformation effects in the theoretical model can better describe the experimental values of α-decay half-lives. In this study, the effect of deformation on α -decay half-lives was investigated using an empirical formula. Within the Wentzel–Kramers–Brillouin (WKB) framework, the Coulomb potential containing the quadrupole deformation of daughter nuclei is considered as the total potential energy of the radioactive system. With some approximations and simplifications, the relationship between the deformation term and α-decay half-life is derived. By incorporating the deformation and angular momentum effects [13, 19, 20], an improved empirical formula was used to investigate α-decay half-lives of even Z-even N, even Z-odd N, odd Z-even N, and odd Z-odd N nuclei with $62 \leqslant Z \leqslant 118$.

Recently, machine learning (ML) algorithms have been used as powerful alternative tools for studying and predicting complex data in nuclear physics [34, 35]. In nuclear structure, ML is used to predict nuclear masses, binding energies, charge radii, etc. [36–49]. ML is a valuable tool for constructing predictive models for nuclear reactions. These models help describe and infer important nuclear reaction data, such as refining the description of reaction data, exploring the initial state of nuclei and reaction geometry, and understanding the reaction mechanism and phase transition [50–53]. Additionally, ML has several advantages in nuclear experiments and the study of dense matter properties [54–59]. Motivated by these advancements, we applied ML to investigate α-decay half-lives of known and unknown nuclei, demonstrating the advantage of this approach in studying α-decay half-lives. In this study, the XGBoost model, which is a powerful and efficient ML algorithm based on gradient boosting decision trees, was employed to further reduce the deviations between experimental and calculated α -decay half-lives of nuclei with $62 \leqslant Z \leqslant 118$. Additionally, we employed XGBoost models along with an improved formula to predict the behavior of unknown superheavy nuclei.

The remainder of this paper is organized as follows. In Sect. 2, a theoretical method for deducing the improved formula and XGBoost model is presented. The results and discussion are presented in Sect. 3. Finally, a brief summary is presented in the final section.

2 Theoretical framework

2.1 Improved formula incorporating deformation effect

In 1928, α-decay was described as a quantum tunneling phenomenon through the potential barrier. In the framework of the semiclassical approximation, the α-decay width (or decay constant) is given by

$$\Gamma \equiv \hbar \ln 2/T_{1/2} = P_0 FP, \tag{1}$$

where P_0 is the preformation probability of the α cluster in the parent nucleus. F is the frequency of the α cluster within the barrier, and P is the probability of transmission through the barrier, which is given by the WKB approximation as follows:

$$P = \exp\left(-\frac{2}{\hbar}\int_{R_{\text{in}}}^{R_{\text{out}}}\sqrt{2\mu|V(r)-Q|}\mathrm{d}r\right). \tag{2}$$

Here, R_{in} is the touching radius, given by $R_{\text{in}} = R_\alpha + R_{\text{d}}$, where R_α and R_{d} are the hard-sphere radii of the α cluster and daughter nuclei, respectively. R_{out} is the classical turning point and is given by $R_{\text{out}} = Z_\alpha Z_{\text{d}} e^2/Q$ [10]. $\mu = A_\alpha A_{\text{d}}/(A_\alpha + A_{\text{d}})$ is the reduced mass of the α-core system. A_α and A_{d} are the mass numbers of the α cluster and daughter nucleus, respectively.

The deformed Coulomb potential [25, 60] is given by

$$V(r) = \frac{Z_\alpha Z_{\text{d}} e^2}{r}\left[1 + \frac{3R_0^2}{5r^2}\beta_2 Y_{20}(\theta)\right], \tag{3}$$

where $R_0 = 1.15A_{\text{d}}^{1/3}$ (fm). Z_α and Z_{d} represent the atomic numbers of the α cluster and daughter nucleus, respectively. β_2 is the quadrupole deformation parameter of the daughter nucleus, and $Y_{20}(\theta)$ is a harmonic function, where θ is the orientation angle of the emitted alpha particle relative to the symmetric axis of the deformed daughter nucleus. Regarding angle θ, previous studies have shown that the penetration probability $P = \int_0^\pi P(\theta)\sin(\theta)\mathrm{d}\theta/2$ is predominantly concentrated around $\theta = 0°$, which is a pole-to-pole state [61–63]. This alignment minimizes the potential barrier, thereby maximizing penetration probability. Therefore, in this study, adopting $\theta = 0°$ simplifies the model while maintaining its accuracy. Combining the above results, probability P can be expressed as follows:

$$P = \exp\left(-\frac{2}{\hbar}\int_{R_{\rm in}}^{R_{\rm out}}\sqrt{2\mu}\sqrt{\left|\left(\frac{Z_\alpha Z_{\rm d}e^2}{r}-Q\right)\left[1+0.162\frac{Z_\alpha Z_{\rm d}e^2 A_{\rm d}^{2/3}\beta_2}{r^3(\frac{Z_\alpha Z_{\rm d}e^2}{r}-Q)}\right]\right|}{\rm d}r\right), \tag{4}$$

By expanding the right-hand term under the square root of Eq. (4) to the first order, we obtain

$$\begin{aligned}\log_{10}P &= -\frac{2}{\hbar\ln 10}\sqrt{2\mu}\left[\int_{R_{\rm in}}^{R_{\rm out}}\left(\frac{Z_\alpha Z_{\rm d}e^2}{r}-Q\right)^{1/2}{\rm d}r\right.\\ &\left.+0.081Z_\alpha Z_d e^2 A_d^{2/3}\beta_2\int_{R_{\rm in}}^{R_{\rm out}}\frac{1}{r^3(\frac{Z_\alpha Z_{\rm d}e^2}{r}-Q)^{1/2}}{\rm d}r\right]\\ &= F_1+F_2,\end{aligned} \tag{5}$$

where F_1 and F_2 are

$$\begin{aligned}F_1 &= -\frac{2}{\hbar\ln 10}\sqrt{2\mu}\int_{R_{\rm in}}^{R_{\rm out}}\left(\frac{Z_\alpha Z_{\rm d}e^2}{r}-Q\right)^{1/2}{\rm d}r,\\ F_2 &= -\frac{81\sqrt{2\mu}Z_\alpha Z_{\rm d}e^2 A_d^{2/3}\beta_2}{500\hbar\ln 10}\int_{R_{\rm in}}^{R_{\rm out}}\frac{1}{r^3\left(\frac{Z_\alpha Z_{\rm d}e^2}{r}-Q\right)^{1/2}}{\rm d}r.\end{aligned} \tag{6}$$

As $R_{\rm out}=Z_\alpha Z_d e^2/Q$, F_1 can be obtained as follows:

$$\begin{aligned}F_1 &= -\frac{2\sqrt{2}e^2}{\hbar\ln 10}\sqrt{\mu}Z_\alpha Z_{\rm d}Q^{-1/2}\\ &\times\left[\arccos(\sqrt{R_{\rm in}/R_{\rm out}})-(R_{\rm in}/R_{\rm out})\sqrt{1-(R_{\rm in}/R_{\rm out})^2}\right].\end{aligned} \tag{7}$$

As the first approximation of the last part of Eq. (7), we obtain

$$F_1 = -\frac{\sqrt{2}\pi e^2}{\hbar\ln 10}\sqrt{\mu}Z_\alpha Z_{\rm d}Q^{-1/2}+\frac{4e\sqrt{2R_{\rm in}}}{\hbar\ln 10}\sqrt{\mu}(Z_\alpha Z_{\rm d})^{1/2}. \tag{8}$$

For α-decay, the variation in $R_{\rm in}$ is minimal. Therefore, $R_{\rm in}$ and $\sqrt{R_{\rm in}}$ are treated as constants here. Equation (8) can be simplified to

$$F_1 = c_1\sqrt{\mu}Z_\alpha Z_{\rm d}Q^{-1/2}+c_2\sqrt{\mu}(Z_\alpha Z_{\rm d})^{1/2}, \tag{9}$$

where c_1 and c_2 are constant coefficients.

Similarly, F_2 can be expressed as

$$\begin{aligned}F_2 &= -\frac{81\sqrt{2\mu}A_{\rm d}^{2/3}\beta_2}{1500\ln 10\hbar Z_\alpha Z_{\rm d}e^2}\left[-\left(\frac{Z_\alpha Z_{\rm d}e^2}{R_{\rm out}}-Q\right)^{3/2}+\left(\frac{Z_\alpha Z_{\rm d}e^2}{R_{\rm in}}-Q\right)^{3/2}\right]\\ &+\frac{81\sqrt{2\mu}A_{\rm d}^{2/3}\beta_2 Q}{500\ln 10\hbar Z_\alpha Z_{\rm d}e^2}\left(-\sqrt{\frac{Z_\alpha Z_{\rm d}e^2}{R_{\rm out}}-Q}+\sqrt{\frac{Z_\alpha Z_{\rm d}e^2}{R_{\rm in}}-Q}\right).\end{aligned} \tag{10}$$

As $R_{\rm out}=Z_\alpha Z_{\rm d}e^2/Q \Rightarrow \frac{Z_\alpha Z_{\rm d}e^2}{R_{\rm out}}-Q=0$, Eq. (10) can be simplified as follows:

$$\begin{aligned}F_2 &= \frac{81\sqrt{2\mu}A_{\rm d}^{2/3}\beta_2}{1500\ln 10\hbar Z_\alpha Z_{\rm d}e^2}\left(\frac{Z_\alpha Z_{\rm d}e^2}{R_{\rm in}}+2Q\right)\\ &\times\left(\frac{Z_\alpha Z_{\rm d}e^2}{R_{\rm in}}\right)^{1/2}\left(1-\frac{QR_{\rm in}}{Z_\alpha Z_{\rm d}e^2}\right)^{1/2}.\end{aligned} \tag{11}$$

Because $\frac{QR_{\rm in}}{Z_\alpha Z_{\rm d}e^2}\ll 1$ and considering the first approximation of the expression in the last part of Eq. (11), we obtain

$$\begin{aligned}F_2 &= \frac{81\sqrt{\mu}}{1500(R_{\rm in})^{3/2}}A_{\rm d}^{2/3}(Z_\alpha Z_{\rm d}e^2)^{1/2}\beta_2\\ &+\frac{81\sqrt{\mu}}{1000(R_{\rm in})^{1/2}}A_{\rm d}^{2/3}(Z_\alpha Z_{\rm d}e^2)^{-1/2}\beta_2 Q\\ &+\frac{161\sqrt{\mu}(R_{\rm in})^{1/2}}{1500}A_{\rm d}^{2/3}(Z_\alpha Z_{\rm d}e^2)^{-3/2}\beta_2 Q^2\\ &= c_3\sqrt{\mu}(Z_\alpha Z_{\rm d})^{1/2}A_{\rm d}^{2/3}\beta_2+c_4\sqrt{\mu}(Z_\alpha Z_{\rm d})^{-1/2}QA_{\rm d}^{2/3}\beta_2\\ &+c_5\sqrt{\mu}(Z_\alpha Z_{\rm d})^{-3/2}Q^2A_{\rm d}^{2/3}\beta_2,\end{aligned} \tag{12}$$

where c_3, c_4, and c_5 are constants. Similarly, as $(Z_\alpha Z_{\rm d})^{-3/2}Q^2A_{\rm d}^{2/3}\ll(Z_\alpha Z_{\rm d})^{-1/2}QA_{\rm d}^{2/3}$, Eq. (12) can be simplified to

$$F_2 = c_3\sqrt{\mu}(Z_\alpha Z_{\rm d})^{1/2}A_{\rm d}^{2/3}\beta_2+c_4\sqrt{\mu}(Z_\alpha Z_{\rm d})^{-1/2}QA_{\rm d}^{2/3}\beta_2. \tag{13}$$

According to Eq. (1), we have

$$\log_{10}T_{1/2} = \log_{10}(\hbar\ln 2/P_0F)-\log_{10}P. \tag{14}$$

In Ref. [10], $P_0=10^{-c_6\sqrt{\mu}(Z_\alpha Z_{\rm d})^{1/2}+c_7}$, where c_6 and c_7 are constants based on experimental results. By combining the results of Eqs. (5), (8), and (13), the right-hand side of Eq. (14) can be expressed as the sum of the following terms: $\sqrt{\mu}Z_\alpha Z_{\rm d}Q^{-1/2}$, $\sqrt{\mu}(Z_\alpha Z_{\rm d})^{1/2}$, $\sqrt{\mu}(Z_\alpha Z_{\rm d})^{1/2}A_{\rm d}^{2/3}\beta_2$, $\sqrt{\mu}(Z_\alpha Z_d)^{-1/2}QA_{\rm d}^{2/3}\beta_2$, and a constant. The equation for α -decay half-lives can be written as

$$\begin{aligned}\log_{10}T_{1/2} &= a\sqrt{\mu}Z_\alpha Z_{\rm d}Q^{-1/2}+b\sqrt{\mu}(Z_\alpha Z_{\rm d})^{1/2}\\ &+c_1\sqrt{\mu}(Z_\alpha Z_{\rm d})^{1/2}A_{\rm d}^{2/3}\beta_2\\ &+c_2\sqrt{\mu}(Z_\alpha Z_{\rm d})^{-1/2}QA_{\rm d}^{2/3}\beta_2+h,\end{aligned} \tag{15}$$

where a, b, c_1, c_2, and h are constants to be determined. Additionally, the influence of angular momentum on α-decay half-lives was studied in Refs. [13, 19, 20]. In this paper, we propose an improved empirical formula to investigate the deformation effect on α-decay half-lives, which is given as

$$\begin{aligned}\log_{10}T_{1/2} = & a\sqrt{\mu}Z_\alpha Z_\mathrm{d}Q^{-1/2} + b\sqrt{\mu}(Z_\alpha Z_\mathrm{d})^{1/2} \\ & + c_1\sqrt{\mu}(Z_\alpha Z_\mathrm{d})^{1/2}A_\mathrm{d}^{2/3}\beta_2 \\ & + c_2\sqrt{\mu}(Z_\alpha Z_\mathrm{d})^{-1/2}QA_\mathrm{d}^{2/3}\beta_2 \\ & + d\,l\,(l+1) + h,\end{aligned} \tag{16}$$

where $T_{1/2}$ (s) is the half-life of α-decay, and Q (MeV) is the α-decay energy. β_2 denotes quadrupole deformation of the daughter nucleus. l is the minimum angular momentum carried away by an α particle [20]. a, b, c_1, c_2, d, and h are constants to be determined.

To compare the calculated results from Eq. (16) with those obtained when the quadrupole deformation of the daughter nuclei is not taken into account, Eq. (16) becomes

$$\begin{aligned}\log_{10}T_{1/2} = & a\sqrt{\mu}Z_\alpha Z_\mathrm{d}Q^{-1/2} + b\sqrt{\mu}(Z_\alpha Z_\mathrm{d})^{1/2} \\ & + d\,l\,(l+1) + h.\end{aligned} \tag{17}$$

2.2 Methodology of eXtreme Gradient Boosting (XGBoost) for α-decay half-lives

The XGBoost algorithm is an ensemble ML algorithm that operates within a gradient boosting framework. It utilizes gradient-boosted decision trees, a technique that significantly enhances performance and speed compared with traditional methods. This algorithm efficiently handles classification, regression, and ranked objective functions and offers a more effective solution than its counterparts, such as Decision Trees (DTs) and Random Forests (RFs). In gradient boosting, a series of weak learners or models are combined to create a robust final model, which is derived by considering the weighted sum of all learned models. XGBoost excels in handling small-to-medium-sized, structured, or low-dimensional datasets, making it suitable for various ML problems.

In contrast to the regularized greedy forest model, XGBoost introduces a unique regularized learning objective. This objective is notable for its simplicity, which enhances the efficiency and effectiveness of the model. The predictive function of XGBoost, a key component of this approach, is expressed as follows:

$$\hat{y}_i = \sum_{k=1}^{K} f_k(x_1), \quad f_k \in \Gamma. \tag{18}$$

In this expression, $\hat{y}_i$ represents the predicted output value for the i-th instance, k denotes the number of regression trees used, and f_k represents the structure of each tree. The feature vector for the i-th sample is denoted by x_i, and Γ represents the space of all possible regression trees.

To address overfitting, a penalty function is introduced to regularize the learning weights as follows:

$$Obj^{(t)} = \left[l\left(y_t - \hat{y}_t^{(t-1)}\right) + g_t f_t(x_t) + \frac{1}{2}h_t f_t^2(x_t)\right] + \Omega(f_t), \tag{19}$$

where $g_i = \partial_{\hat{y}}(t-1)l\left(y_i, \hat{y}^{(t-1)}\right)$ and $h_i = \partial^2_{\hat{y}^{(t-1)}}l\left(y_i - \hat{y}^{(k-1)}\right)$ are the first- and second-order gradient statistics of the loss function, respectively. The constant term is eliminated, yielding the objective function for the i-th step as follows:

$$Obj^{(t)} = \sum_{t=1}^{n}\left[g_i f_t(x_l) + \frac{1}{2}h_t f_t^2(x_l)\right] + \Omega(f_t). \tag{20}$$

The parameters in Eq. (20) can be updated continuously until the stopping criteria are satisfied. Further details on XGBoost can be found in Ref. [64].

In the context of α-decay half-lives, XGBoost considers the experimental α-decay half-lives as the ground truth and learns from the residuals between these data and the predictions made by the empirical formulas in Eqs. (17) and (16). This residual-based learning allows the model to implicitly account for missing physical factors, such as shell effects. The input features include the quadrupole deformation values (β_2) of the daughter nucleus derived from the WS4 and FRDM models, along with the reduced mass (μ) of the α-core system, proton numbers (Z_d, Z_c) of the daughter nucleus and α cluster, α-decay energy, and other relevant nuclear properties. These features allow the model to identify complex correlations, such as those related to magic and sub-magic numbers, that are not encoded in empirical formulas. Owing to these advantages, XGBoost enhances the ability to capture nonlinear relationships and systematic discrepancies, particularly in regions where empirical formulas typically fail, such as near-shell closures. The XGBoost model is formulated as

$$R_n = T_{1/2}^{\mathrm{exp}}(x_n) - T_{1/2}^{\mathrm{cal}}(x_n) = \sum_{k=1}^{K} f_k(x_1), \quad f_k \in \Gamma, \tag{21}$$

where R_n represents the residuals for the n-th nucleus, $T_{1/2}^{\mathrm{exp}}(x_n)$ is the experimental α-decay half-life, and $T_{1/2}^{\mathrm{cal}}(x_n)$ is the calculated α-decay half-life obtained using the empirical formula. The XGBoost model, through its sophisticated learning mechanism, is trained to minimize these residuals, thereby improving the alignment between theoretical predictions and experimental data. The optimization of model parameters, as described in Eq. (20), focuses on minimizing

Table 1 Parameter values of Eq. (17)

Nuclei	a	b	d	h
Even Z-even N	0.4052	−1.5073	0	−12.1265
Even Z-odd N	0.4101	−1.5008	0.04556	−12.6194
Odd Z-even N	0.4181	−1.4863	0.05270	−14.0310
Odd Z-odd N	0.4163	−1.4782	0.04998	−13.6438

the residuals to achieve the highest possible prediction accuracy.

3 Results and discussion

3.1 Nuclear deformation effect on α-decay half-lives with improved formula

In this study, the α-decay half-lives of 675 nuclei were extracted, including 183 even-even nuclei, 188 even Z-odd N nuclei, 178 odd Z-even N nuclei, and 126 odd Z-odd N nuclei. The experimental α-decay half-lives, spins, and parities were obtained from the evaluated properties table NUBASE2020 [65], and the α-decay energy was obtained from the evaluated atomic mass table AME2020 [66]. The quadrupole deformation values of the daughter nuclei in Eq. (16) were obtained from the WS4 [67] and FRDM [68] mass models. For different nuclei types, the parameters in Eqs. (17) and (16) were obtained by fitting the experimental α-decay half-lives. The fitting coefficients are listed in Tables 1, 2 and 3. Note that the parameters in Table 1 are fitted by the experimental α-decay half-lives of the nuclei with an absolute quadrupole deformation of less than 0.1. The parameters in Tables 2 and 3 were fitted using the experimental α-decay half-lives of all nuclei.

To precisely compare the different formulas, the root mean square deviation (RMSD) of the nuclei can be calculated as follows:

$$\sigma = \sqrt{\sum_{i=1}^{n} (\log_{10} T_{1/2}^{\mathrm{cal}} - \log_{10} T_{1/2}^{\mathrm{exp}})_i^2 / n}, \tag{22}$$

where $T_{1/2}^{\mathrm{cal}}$ is the calculated α-decay half-life, and $T_{1/2}^{\mathrm{exp}}$ is the experimental α-decay half-life. The RMSDs for the different formulas are listed in Table 4. Using the quadrupole deformation values of the daughter nuclei in Eq. (16), taken from the WS4 and FRDM models, the corresponding σ values are denoted as σ_2 and σ_3, respectively. Additionally, σ_1, σ_4, and σ_5 represent the σ values between the experimental data and calculated results obtained from Eq. (17) and other formulas [8, 13], respectively.

When the quadrupole deformation of the daughter nuclei in Eq. (16) is taken from the WS4 mass model, the σ values decrease from 0.406 to 0.363 for even Z-even N nuclei, from 0.475 to 0.445 for even Z-odd N nuclei, from 0.469 to 0.412 for odd Z-even N nuclei, and from 0.472 to 0.432 for odd Z-odd N nuclei. A similar trend was observed when the quadrupole deformation values were taken from the FRDM model. Among all subsets, the σ values for even Z-even N nuclei were the lowest, with σ_1, σ_2, and σ_3 values of 0.406, 0.363, and 0.368, respectively. This can be attributed to the fact that in the α-decay of even Z-even N nuclei, the angular momentum l carried away by the α particle is always zero, eliminating the ambiguity in determining l, which is not true for other subsets. For the total dataset, the σ_2 and σ_3 values, when compared with the σ_1 value from Eq. (17), decrease from 0.456 to 0.413 and 0.415, respectively. From the σ values, including deformation effects in the empirical formula

Table 2 Parameter values of Eq. (16) obtained by fitting the experimental α-decay half-lives, where the values of the quadrupole deformation of the daughter nuclei were taken from the WS4 model [67]

Nuclei	a	b	c_1	c_2	d	h
Even Z-even N	0.4124	−1.5354	−0.0072	0.1536	0	−12.2610
Even Z-odd N	0.4138	−1.4461	−0.0032	0.0693	0.0453	−14.4611
Odd Z-even N	0.4148	−1.4657	−0.0059	0.1316	0.0507	−14.1217
Odd Z-odd N	0.4145	−1.4866	0.0074	−0.0178	0.0511	−13.2610

Table 3 Same as Table 2, but the values of the quadrupole deformation of the daughter nuclei were taken from the FRDM model [68]

Nuclei	a	b	c_1	c_2	d	h
Even Z-even N	0.4117	−1.5500	−0.0067	0.1527	0	−11.8213
Even Z-odd N	0.4140	−1.4474	−0.0031	0.0647	0.0453	−14.4561
Odd Z-even N	0.4146	−1.4723	−0.0061	0.1420	0.0511	−13.9411
Odd Z-odd N	0.4176	−1.4695	−0.0020	0.0946	0.0516	−14.0118

Table 4 Root mean square deviations between experimental α-decay half-lives and the calculated results obtained by Eqs. (17), (16), and other formulas [8, 13]. σ_1, σ_4, and σ_5 represent the σ deviations between the experimental data and calculated results from Eq. (17) and other formulas [8, 13], respectively. With the quadrupole deformation values of the daughter nuclei in Eq. (16) taken from the WS4 and FRDM models, the corresponding σ deviations are denoted as σ_2 and σ_3, respectively

	Eq. (17)	Eq. (16)		Ref. [8]	Ref. [13]	
Nuclei	σ_1	σ_2	σ_3	σ_4	σ_5	No. of nuclei
Even Z-even N	0.406	0.363	0.368	0.376	0.375	183
Even Z-odd N	0.475	0.445	0.445	0.668	0.457	188
Odd Z-even N	0.469	0.412	0.409	0.653	0.425	178
Odd Z-odd N	0.472	0.432	0.439	0.634	0.475	126
Total	0.456	0.413	0.415	0.589	0.428	675

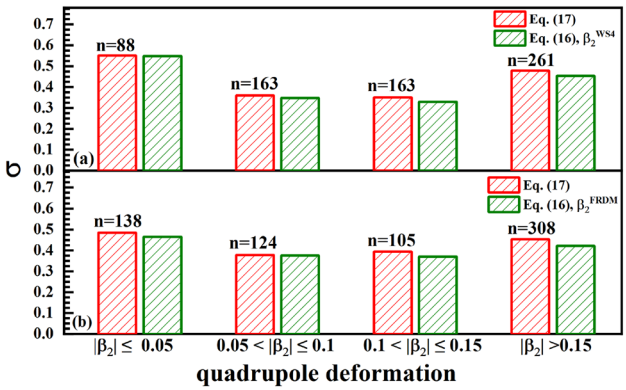

Fig. 1 (Color online) Root mean square deviations of Eqs. (17) and (16) for nuclei across different deformation regions of the daughter nuclei, with the quadrupole deformation values of daughter nuclei taken from WS4 (a) and FRDM (b) models. The horizontal axis represents the range of deformation values for the daughter nuclei, whereas the vertical axis indicates the root mean square values for nuclei within each deformation range. n represents the number of nuclei present in each deformation interval

does not significantly improve describing experimental α -decay half-lives.

Additionally, by fixing the parameters a, b, d, and h in Eq. (17), the deformation-related parameters c_1 and c_2 are independently fitted by the experimental α-decay half-lives. Using this approach, Eq. (16) produces $\sigma = 0.419$ and 0.421 with the quadrupole deformation values obtained from WS4 and FRDM, respectively. Compared with the values of σ_2 and σ_3 shown in Table 4, their σ values are higher. Hence, the results calculated from Eq. (16), where the parameters of Eq. (16) are fitted using the experimental α-decay half-lives of all nuclei, will be used in the subsequent discussions on XGBoost optimization and the prediction of α-decay half-lives for superheavy nuclei.

In Fig. 1, the σ deviations of Eqs. (17) and (16) across different quadrupole deformation regions are presented, with the deformation values derived from the WS4 and FRDM models, respectively. For nuclei with small deformations ($|\beta_2| \leq 0.05$), the difference between the two formulas (Eqs. (17) and (16)) is negligible. This suggests that the deformation effect is minimal in this range. In the intermediate deformation range ($0.05 < |\beta_2| \leq 0.15$), the σ values in Eq. (16) are slightly lower than those in Eq. (17), indicating a better consistency with the experimental data in this range. For nuclei with large deformation ($|\beta_2| > 0.15$), the deformation-inclusive equation (Eq. 16) shows a further reduction in the σ values, indicating that considering deformation improves the agreement with experimental data for highly deformed nuclei. Overall, the σ deviations in Eq. (16) are consistently smaller than those in Eq. (17) across all deformation ranges, as shown in Fig. 1a, b. Although deformation has little impact on near-spherical nuclei, it becomes increasingly relevant as deformation increases. Although the improved formula does not significantly reduce the overall σ value, it achieves better consistency with experimental data for highly deformed nuclei, with minimal effect on less deformed nuclei.

Using the RMSD as an indicator of the accuracy of the formula provides only a rough estimate of its performance. For a more detailed insight, Fig. 2 presents the logarithmic deviations between the experimental data and the results calculated using Eqs. (17) and (16). In Fig. 2a, the black circles and red stars represent the deviations for Eqs. (17) and (16), respectively, using the deformation values from the WS4 model [67]. Similarly, Fig. 2b presents the same analysis using the deformation values from the FRDM model [68]. Points closer to zero indicate better agreement with experimental data, and evidently, the deviations of Eq. (16) (red stars) are more concentrated near zero than those of Eq. (17) (black circles) for both models. A notable feature in Fig. 2 is the large deviations observed near neutron numbers $N = 126$ and $N = 152$, where both formulas exhibit significant discrepancies from the experimental data. Previous studies identified $N = 126$ and $N = 152$ as magic and sub-magic numbers, respectively [69–71]. These deviations can be attributed to shell effects associated with these neutron numbers, which are

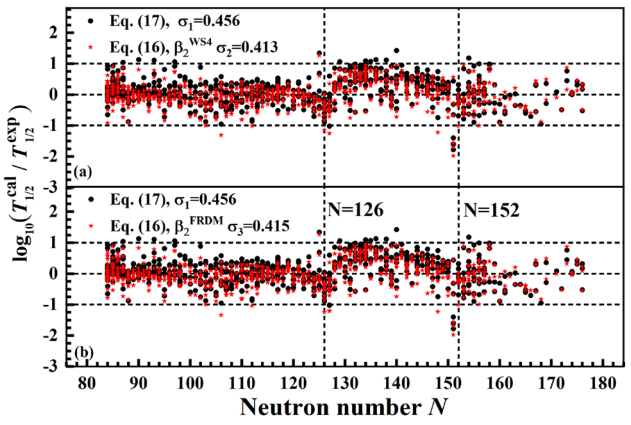

Fig. 2 (Color online) Logarithmic differences between the experimental α-decay half-lives and calculated results obtained by Eqs. (17) and (16), with values of the quadrupole deformation of the daughter nuclei taken from the WS4 (a) and FRDM (b) models, respectively. The dashed lines represent the neutron numbers $N = 126$, 152, and the deviations of the decimal logarithms of $T^{\rm cal}_{1/2}/T^{\rm exp}_{1/2}$ are 0, –1, and 1, respectively

not explicitly accounted for in either Eq. (17) or (16). To address this issue, in the following sections, we explore using the XGBoost algorithm to further reduce the σ values of empirical formulas, including nuclei near the magic and sub-magic numbers.

To gain further insight into the deformation effect on α -decay half-lives, we compared the improved formula of Eq. (16) with other formulas [8, 13]. The experimental data used in this study differ from those in Refs. [8] and [13]. The parameters of the empirical formulas in Refs. [8, 13] were recalibrated using the experimental data obtained in this study. This recalibration resulted in σ values of 0.589 and 0.428, respectively, which were lower than the original σ values of 0.779 and 0.429 with the parameters obtained from Refs. [8] and Ref. [13], respectively. The recalibrated σ values for the four subsets and total dataset are displayed in the fifth and sixth columns of Table 4, respectively. As indicated in the table, the improved formula of Eq. (16) exhibits smaller σ values for the entire set of data than those of the other formulas [8, 13]. This indicates that the improved formula, which incorporates the deformation effect, can be used to study α-decay half-lives.

3.2 Study on α-decay half-lives with eXtreme gradient boosting

In this study, we built three XGBoost models to further improve the prediction accuracy of α-decay half-lives, denoted as XGBoost1, XGBoost2, and XGBoost3. For the XGBoost2 and XGBoost3 models, the quadrupole deformation values of the daughter nuclei were obtained from the WS4 and FRDM models, respectively. Additionally, in the XGBoost models, the physical terms of Eqs. (17) and (16) were used as inputs, and the residuals between the calculated and experimental α-decay half-lives served as the output.

The experimental data for 675 nuclei were extracted and divided into two sets: the training set (540 nuclei) and testing set (135 nuclei). The corresponding σ values calculated using the formulas and XGBoost1, XGBoost2, and XGBoost3 models are presented in Table 5. The σ values of the XGBoost1, XGBoost2, and XGBoost3 models show an obvious decrease compared with those of Eqs. (17) and (16) for the training and testing sets. For the entire set, the σ values of XGBoost1, XGBoost2, and XGBoost3 models reduced from 0.456 to 0.316, from 0.413 to 0.295, and from 0.415 to 0.302, respectively. This indicates that XGBoost models can further reduce the deviation between the calculated and experimental α-decay half-lives.

The deviations between the experimental data and results calculated using the empirical formula (blue circles) and XGBoost models (red stars) are illustrated in Fig. 3. As shown in Fig. 3, the majority of blue circles are scattered in the range of $\pm$ 1, suggesting larger deviations. By contrast, most red stars fall within the range of $\pm$ 0.5, indicating a closer alignment to the zero line. For nuclei near the neutron magic number $N = 126$ and sub-magic number $N = 152$, the deviations obtained by XGBoost models are smaller than those from the empirical formulas in Eqs. (17) and (16). To further quantify these differences, Fig. 4 shows the σ values in Eq. (17), Eq. (16), and the XGBoost models (XGBoost1, XGBoost2, and XGBoost3) for nuclei with $N = 125, 126, 127, 151, 152$, and 153. The comparison shows that the σ values for the XGBoost models were reduced from 0.623 to 0.562, from 0.685 to 0.533, and from 0.687 to 0.543, respectively, indicating better consistency with the experimental data than

Table 5 Root mean square deviations between experimental α-decay half-lives and calculated results using Eqs. (17), (16), XGBoost1, XGBoost2, and XGBoost3 for training, testing, and entire sets

	Inputs	σ (training set)	σ (testing set)	σ (entire set)
Equation (17)	–	0.462	0.418	0.456
XGBoost1	(Q_α, μ, Z_c, Z_d, l)	0.310	0.346	0.316
(Eq. (16), $\beta_2^{\rm WS4}$)	–	0.427	0.345	0.413
XGBoost2	(Q_α, μ, Z_c, Z_d, l, $\beta_2^{\rm WS4}$)	0.288	0.318	0.295
(Eq. (16), $\beta_2^{\rm FRDM}$)	–	0.430	0.345	0.415
XGBoost3	(Q_α, μ, Z_c, Z_d, l, $\beta_2^{\rm FRDM}$)	0.301	0.308	0.302

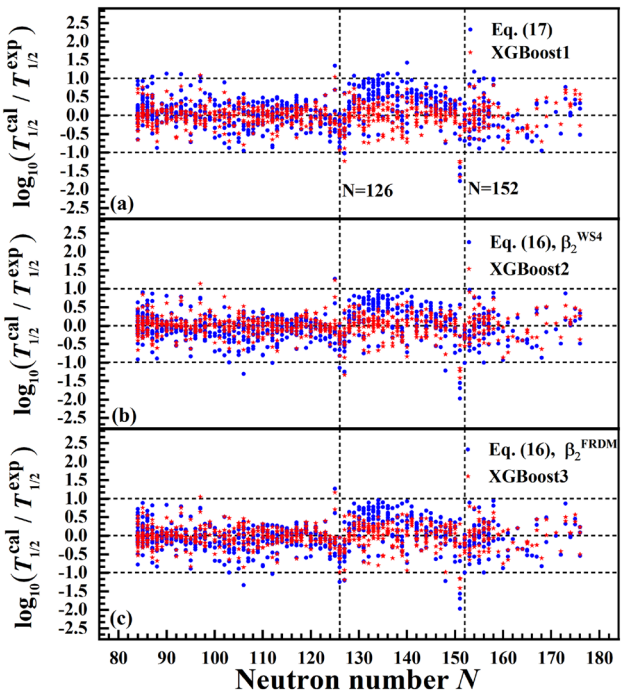

Fig. 3 (Color online) Logarithmic differences between the experimental data and calculated α-decay half-lives using **a** Eq. (17) and XGBoost1, **b** Eq. (16) and XGBoost2, and **c** Eq. (16) and XGBoost3. The values of quadrupole deformation of the daughter nuclei in Eq. (16) are taken from the WS4 and FRDM models, respectively. The dashed lines represent the deviation of the decimal logarithms of $T^{cal}_{1/2}/T^{exp}_{1/2}$ of 0, –1, and 1, respectively

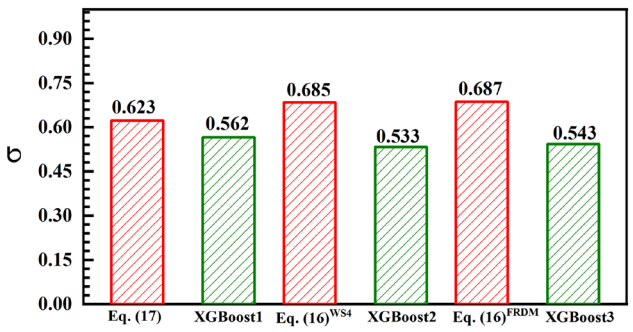

Fig. 4 (Color online) Root mean square deviations between the experimental data and calculated α-decay half-lives using Eqs. (17), (16), XGBoost1, XGBoost2, and XGBoost3 models for the 53 nuclei at N= 125, 126, 127, 151, 152, and 153

with the empirical formulas. For these nuclei, the larger deviations of the empirical formulas can be attributed to their lack of consideration of shell effects. By contrast, the XGBoost models effectively capture missing physical effects, such as shell effects, by learning from the residuals between the empirical formulas and experimental data. Consequently, the XGBoost models further reduced the deviations for nuclei near the neutron magic number $N = 126$ and sub-magic number $N = 152$, providing more accurate predictions.

3.3 Predictions of α-decay half-lives of nuclei with Z = 117, 118, 119, and 120

Using the improved formula of Eq. (16), along with the XGBoost2 and XGBoost3 models, we predict the α-decay half-lives of SHN with Z = 117, 118, 119, and 120. In Table 6, the first column lists the α-decay, followed by the α -decay energy and quadrupole deformation of the daughter nuclei (columns 2-5), obtained from WS4 [67] and FRDM [68] mass models, respectively. The spin and parity values of the parent and daughter nuclei in the nuclear ground state were taken from Ref. [72]. Because of challenges in determining the spin and parity of doubly odd SHN, we assume that the minimum angular momentum l carried away by the α particle is zero. As shown in the eighth to last columns, the decimal logarithms of α-decay half-lives, calculated using the improved formula Eq. (16), are shown as $\log_{10}T^{Cal1}_{1/2}$ and $\log_{10}T^{Cal2}_{1/2}$, with the values of the quadrupole deformation taken from WS4 and FRDM models, respectively. Additionally, $\log_{10}T^{XGBoost1}_{1/2}$ and $\log_{10}T^{XGBoost2}_{1/2}$ were calculated using the XGBoost2 and XGBoost3 models, respectively.

The calculated α-decay half-lives of the nuclei with Z = 117, 118, 119, and 120 are plotted in Fig. 5, respectively. As shown in Fig. 5, the calculated α-decay half-lives for ^{293}Ts, obtained using the improved formula ($\log_{10}T^{Cal1}_{1/2}$ and $\log_{10}T^{Cal2}_{1/2}$) and the XGBoost models ($\log_{10}T^{XGBoost1}_{1/2}$ and

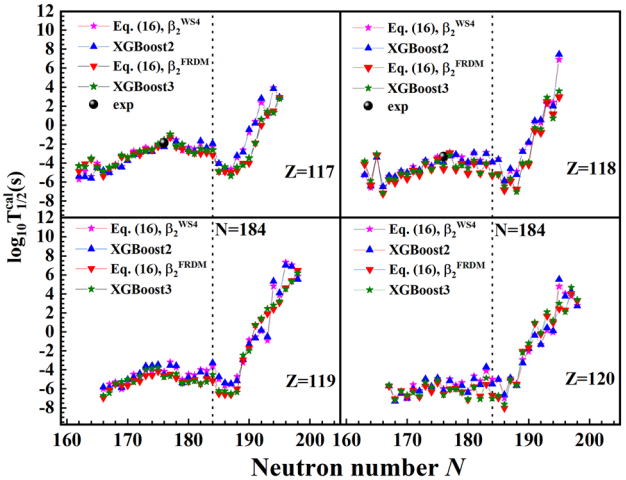

Fig. 5 (Color online) Logarithms of α-decay half-lives of nuclei with Z = 117, 118, 119, and 120 using Eq. (16), XGBoost2, and XGBoost3 with Q_α obtained by the WS4 [67] and FRDM [68] nuclear mass table. The black dashed lines denote the neutron number N = 184

Table 6 α-decay half-lives of nuclei with $Z = 117$, 118, 119, and 120, with the α-decay energy and quadrupole deformation obtained by the WS4 [67] and FRDM [68] mass models, respectively. The logarithms of α-decay half-lives were calculated using Eq. (16), denoted by $\log_{10}T_{1/2}^{\mathrm{Cal1}}$ and $\log_{10}T_{1/2}^{\mathrm{Cal2}}$, with the values of the quadrupole deformation obtained from the WS4 and FRDM models, respectively. Additionally, $\log_{10}T_{1/2}^{\mathrm{XGBoost1}}$ and $\log_{10}T_{1/2}^{\mathrm{XGBoost2}}$ were calculated using the XGBoost2 and XGBoost3 models, respectively

α transition	Q_α^{WS4} (MeV)	Q_α^{FRDM} (MeV)	β_2^{WS4}	β_2^{FRDM}	l	$\log_{10}T_{1/2}^{\mathrm{Cal1}}$	$\log_{10}T_{1/2}^{\mathrm{XGBoost1}}$	$\log_{10}T_{1/2}^{\mathrm{Cal2}}$	$\log_{10}T_{1/2}^{\mathrm{XGBoost2}}$
$^{279}\mathrm{Ts}\rightarrow{}^{275}\mathrm{Mc}$	13.36	12.97	0.1792	0.198	2	−5.734	−5.391	−4.904	−4.306
$^{280}\mathrm{Ts}\rightarrow{}^{276}\mathrm{Mc}$	13.42	12.79	0.1825	0.198	0	−4.876	−5.454	−4.097	−4.388
$^{281}\mathrm{Ts}\rightarrow{}^{277}\mathrm{Mc}$	13.21	12.32	0.1822	0.198	2	−5.440	−5.619	−3.633	−3.525
$^{282}\mathrm{Ts}\rightarrow{}^{278}\mathrm{Mc}$	13.00	12.59	0.1803	0.032	0	−4.039	−4.495	−4.376	−4.512
$^{283}\mathrm{Ts}\rightarrow{}^{279}\mathrm{Mc}$	12.86	12.96	−0.0141	−0.011	2	−5.150	−4.800	−5.402	−4.909
$^{284}\mathrm{Ts}\rightarrow{}^{280}\mathrm{Mc}$	12.66	12.65	−0.0239	0.021	0	−5.023	−5.008	−4.548	−4.447
$^{285}\mathrm{Ts}\rightarrow{}^{281}\mathrm{Mc}$	12.42	12.45	0.0404	0.032	2	−4.123	−4.319	−4.240	−4.287
$^{286}\mathrm{Ts}\rightarrow{}^{282}\mathrm{Mc}$	12.24	12.18	−0.0573	0.064	0	−4.385	−4.455	−3.357	−3.201
$^{287}\mathrm{Ts}\rightarrow{}^{283}\mathrm{Mc}$	12.02	12.11	−0.0719	0.064	2	−3.403	−3.743	−3.441	−3.446
$^{288}\mathrm{Ts}\rightarrow{}^{284}\mathrm{Mc}$	11.95	12.01	0.0618	0.064	0	−2.743	−3.121	−2.976	−3.170
$^{289}\mathrm{Ts}\rightarrow{}^{285}\mathrm{Mc}$	11.96	11.98	0.0707	0.064	2	−3.076	−2.888	−3.152	−2.743
$^{290}\mathrm{Ts}\rightarrow{}^{286}\mathrm{Mc}$	11.81	11.85	0.0676	0.075	0	−2.364	−2.774	−2.567	−2.752
$^{291}\mathrm{Ts}\rightarrow{}^{287}\mathrm{Mc}$	11.69	11.75	−0.1016	0.064	2	−2.647	−2.806	−2.630	−2.549
$^{292}\mathrm{Ts}\rightarrow{}^{288}\mathrm{Mc}$	11.72	11.71	0.0654	0.064	0	−2.178	−2.141	−2.282	−2.021
$^{293}\mathrm{Ts}\rightarrow{}^{289}\mathrm{Mc}$	11.60	11.40	0.062	0.064	2	−2.255	−2.294	−1.805	−1.565
$^{294}\mathrm{Ts}\rightarrow{}^{290}\mathrm{Mc}$	11.35	11.29	0.0544	0.053	0	−1.363	−1.204	−1.306	−0.965
$^{295}\mathrm{Ts}\rightarrow{}^{291}\mathrm{Mc}$	11.27	11.55	−0.0729	−0.042	2	−1.570	−1.741	−2.312	−2.218
$^{296}\mathrm{Ts}\rightarrow{}^{292}\mathrm{Mc}$	11.48	11.64	−0.062	−0.042	0	−2.678	−2.359	−2.511	−2.007
$^{297}\mathrm{Ts}\rightarrow{}^{293}\mathrm{Mc}$	11.59	11.76	−0.0555	−0.021	2	−2.363	−2.621	−2.786	−2.712
$^{298}\mathrm{Ts}\rightarrow{}^{294}\mathrm{Mc}$	11.49	11.86	−0.0392	−0.021	0	−2.523	−2.811	−2.956	−3.001
$^{299}\mathrm{Ts}\rightarrow{}^{295}\mathrm{Mc}$	11.43	11.86	−0.0334	−0.021	2	−1.951	−1.686	−3.021	−2.512
$^{300}\mathrm{Ts}\rightarrow{}^{296}\mathrm{Mc}$	11.53	11.88	−0.0319	−0.011	0	−2.536	−2.401	−2.964	−2.679
$^{301}\mathrm{Ts}\rightarrow{}^{297}\mathrm{Mc}$	11.59	11.93	−0.0276	−0.011	2	−2.323	−1.957	−3.166	−2.612
$^{302}\mathrm{Ts}\rightarrow{}^{298}\mathrm{Mc}$	12.20	12.75	−0.0154	−0.011	0	−3.959	−4.070	−4.891	−4.898
$^{303}\mathrm{Ts}\rightarrow{}^{299}\mathrm{Mc}$	12.75	12.74	−0.0087	0	2	−4.918	−4.509	−4.918	−4.417
$^{304}\mathrm{Ts}\rightarrow{}^{300}\mathrm{Mc}$	12.52	12.82	−0.0145	0	0	−4.642	−5.088	−4.988	−5.366
$^{305}\mathrm{Ts}\rightarrow{}^{301}\mathrm{Mc}$	12.06	12.69	−0.0214	0	2	−3.413	−3.229	−4.813	−4.475
$^{306}\mathrm{Ts}\rightarrow{}^{302}\mathrm{Mc}$	11.58	12.40	−0.0277	0.011	0	−2.629	−2.864	−4.046	−4.195
$^{307}\mathrm{Ts}\rightarrow{}^{303}\mathrm{Mc}$	10.90	12.24	−0.0466	0.011	1	−0.785	−0.473	−4.026	−3.480
$^{308}\mathrm{Ts}\rightarrow{}^{304}\mathrm{Mc}$	10.33	11.49	−0.0575	0.021	0	0.375	0.186	−1.908	−1.883
$^{309}\mathrm{Ts}\rightarrow{}^{305}\mathrm{Mc}$	9.99	10.80	−0.1822	−0.011	3	2.346	2.788	−0.048	0.579
$^{310}\mathrm{Ts}\rightarrow{}^{306}\mathrm{Mc}$	9.73	10.37	−0.1855	0.044	0	0.974	1.273	1.115	1.415
$^{311}\mathrm{Ts}\rightarrow{}^{307}\mathrm{Mc}$	9.42	10.15	−0.2	0.054	2	3.924	3.842	1.488	1.311
$^{312}\mathrm{Ts}\rightarrow{}^{308}\mathrm{Mc}$	9.05	9.78	−0.2111	0.065	0	2.968	2.905	2.923	2.805
$^{281}\mathrm{Og}\rightarrow{}^{277}\mathrm{Lv}$	13.77	13.15	0.1787	0.186	5	−5.274	−5.254	−4.129	−3.825
$^{282}\mathrm{Og}\rightarrow{}^{278}\mathrm{Lv}$	13.49	13.12	0.1799	0	0	−6.582	−6.431	−6.335	−5.864
$^{283}\mathrm{Og}\rightarrow{}^{279}\mathrm{Lv}$	13.32	13.20	0.1792	0.032	7	−3.262	−3.395	−3.171	−3.062
$^{284}\mathrm{Og}\rightarrow{}^{280}\mathrm{Lv}$	13.21	13.56	−0.0262	0	0	−6.475	−6.502	−7.191	−7.133
$^{285}\mathrm{Og}\rightarrow{}^{281}\mathrm{Lv}$	13.05	13.24	0.0363	0.032	0	−5.399	−5.362	−5.788	−5.692
$^{286}\mathrm{Og}\rightarrow{}^{282}\mathrm{Lv}$	12.89	13.05	0.0479	0.053	0	−5.698	−5.463	−6.066	−5.741
$^{287}\mathrm{Og}\rightarrow{}^{283}\mathrm{Lv}$	12.77	12.96	0.056	0.064	0	−4.820	−4.884	−5.204	−5.084
$^{288}\mathrm{Og}\rightarrow{}^{284}\mathrm{Lv}$	12.59	12.86	−0.0765	0.064	0	−5.257	−5.026	−5.662	−5.215
$^{289}\mathrm{Og}\rightarrow{}^{285}\mathrm{Lv}$	12.56	12.76	0.0711	0.075	0	−4.370	−4.664	−4.787	−4.914
$^{290}\mathrm{Og}\rightarrow{}^{286}\mathrm{Lv}$	12.57	12.68	0.075	0.075	0	−5.008	−4.771	−5.273	−4.896
$^{291}\mathrm{Og}\rightarrow{}^{287}\mathrm{Lv}$	12.39	12.55	0.075	0.075	2	−3.728	−3.781	−4.075	−3.934

Table 6 (continued)

α transition	Q_α^{WS4} (MeV)	Q_α^{FRDM} (MeV)	β_2^{WS4}	β_2^{FRDM}	l	$\log_{10}T_{1/2}^{\mathrm{Cal1}}$	$\log_{10}T_{1/2}^{\mathrm{XGBoost1}}$	$\log_{10}T_{1/2}^{\mathrm{Cal2}}$	$\log_{10}T_{1/2}^{\mathrm{XGBoost2}}$
$^{292}\mathrm{Og}\rightarrow{}^{288}\mathrm{Lv}$	12.21	12.39	0.0735	0.075	0	−4.248	−4.392	−4.671	−4.676
$^{293}\mathrm{Og}\rightarrow{}^{289}\mathrm{Lv}$	12.21	12.34	0.0711	0.075	2	−3.344	−3.807	−3.624	−3.867
$^{294}\mathrm{Og}\rightarrow{}^{290}\mathrm{Lv}$	12.17	12.37	0.0687	0.064	0	−4.163	−3.963	−4.649	−4.223
$^{295}\mathrm{Og}\rightarrow{}^{291}\mathrm{Lv}$	11.88	11.92	0.0617	0.064	0	−2.857	−3.270	−2.962	−3.192
$^{296}\mathrm{Og}\rightarrow{}^{292}\mathrm{Lv}$	11.73	12.28	0.0532	−0.073	0	−3.176	−3.102	−4.703	−4.420
$^{297}\mathrm{Og}\rightarrow{}^{293}\mathrm{Lv}$	12.08	12.38	−0.0789	−0.063	0	−3.385	−3.801	−4.055	−4.241
$^{298}\mathrm{Og}\rightarrow{}^{294}\mathrm{Lv}$	12.16	12.49	−0.0651	−0.042	0	−4.279	−3.902	−5.112	−4.549
$^{299}\mathrm{Og}\rightarrow{}^{295}\mathrm{Lv}$	12.02	12.51	−0.0507	−0.021	2	−2.968	−2.939	−4.044	−3.709
$^{300}\mathrm{Og}\rightarrow{}^{296}\mathrm{Lv}$	11.93	12.51	−0.0441	−0.011	0	−3.733	−3.926	−5.093	−5.066
$^{301}\mathrm{Og}\rightarrow{}^{297}\mathrm{Lv}$	12.00	12.56	−0.0396	0	2	−2.903	−3.012	−4.138	−4.000
$^{302}\mathrm{Og}\rightarrow{}^{298}\mathrm{Lv}$	12.02	12.62	−0.0336	0	0	−3.923	−3.913	−5.305	−5.175
$^{303}\mathrm{Og}\rightarrow{}^{299}\mathrm{Lv}$	12.58	13.38	−0.0197	0	4	−3.566	−3.666	−5.179	−5.227
$^{304}\mathrm{Og}\rightarrow{}^{300}\mathrm{Lv}$	13.10	13.39	−0.0136	0	0	−6.232	−5.888	−6.863	−6.450
$^{305}\mathrm{Og}\rightarrow{}^{301}\mathrm{Lv}$	12.89	13.45	−0.0188	0	2	−4.837	−4.617	−5.950	−5.621
$^{306}\mathrm{Og}\rightarrow{}^{302}\mathrm{Lv}$	12.46	13.35	−0.0264	0	0	−4.906	−5.248	−6.785	−7.042
$^{307}\mathrm{Og}\rightarrow{}^{303}\mathrm{Lv}$	11.90	12.57	−0.0397	0.011	2	−2.690	−2.802	−4.152	−4.016
$^{308}\mathrm{Og}\rightarrow{}^{304}\mathrm{Lv}$	11.18	12.10	−0.0484	0	0	−1.893	−1.810	−4.168	−3.900
$^{309}\mathrm{Og}\rightarrow{}^{305}\mathrm{Lv}$	10.70	11.07	−0.0584	0.022	2	0.359	0.422	−0.626	−0.288
$^{310}\mathrm{Og}\rightarrow{}^{306}\mathrm{Lv}$	10.41	10.74	−0.1812	0.044	0	0.268	0.534	−0.795	−0.415
$^{311}\mathrm{Og}\rightarrow{}^{307}\mathrm{Lv}$	10.08	9.98	−0.2049	−0.042	2	2.177	2.561	2.441	2.917
$^{312}\mathrm{Og}\rightarrow{}^{308}\mathrm{Lv}$	9.74	10.05	−0.207	0.055	0	2.406	1.999	1.131	0.706
$^{313}\mathrm{Og}\rightarrow{}^{309}\mathrm{Lv}$	8.63	9.72	−0.2135	0.066	0	6.890	7.432	2.925	3.570
$^{285}119\rightarrow{}^{281}\mathrm{Ts}$	13.60	14.06	0.0304	0	2	−5.998	−5.813	−6.979	−6.712
$^{286}119\rightarrow{}^{282}\mathrm{Ts}$	13.42	13.75	0.0401	0.043	0	−5.494	−5.914	−6.112	−6.442
$^{287}119\rightarrow{}^{283}\mathrm{Ts}$	13.26	13.37	0.0524	0.064	2	−5.288	−5.535	−5.497	−5.466
$^{288}119\rightarrow{}^{284}\mathrm{Ts}$	13.20	13.57	−0.0751	0.075	0	−6.040	−5.900	−5.620	−5.264
$^{289}119\rightarrow{}^{285}\mathrm{Ts}$	13.13	13.47	−0.0845	0.075	2	−5.310	−5.027	−5.656	−5.025
$^{290}119\rightarrow{}^{286}\mathrm{Ts}$	13.04	13.31	0.0721	0.075	0	−4.465	−4.804	−5.117	−5.316
$^{291}119\rightarrow{}^{287}\mathrm{Ts}$	13.02	13.24	0.0773	0.075	2	−4.773	−4.409	−5.215	−4.657
$^{292}119\rightarrow{}^{288}\mathrm{Ts}$	12.87	13.08	0.0776	0.086	0	−4.073	−3.611	−4.610	−4.013
$^{293}119\rightarrow{}^{289}\mathrm{Ts}$	12.69	12.92	0.0746	0.075	2	−4.099	−3.580	−4.581	−3.869
$^{294}119\rightarrow{}^{290}\mathrm{Ts}$	12.70	12.85	0.0739	0.075	0	−3.731	−3.474	−4.187	−3.790
$^{295}119\rightarrow{}^{291}\mathrm{Ts}$	12.73	12.94	0.0732	0.075	2	−4.191	−4.541	−4.620	−4.776
$^{296}119\rightarrow{}^{292}\mathrm{Ts}$	12.45	12.98	0.0733	0.075	0	−3.191	−3.550	−4.452	−4.671
$^{297}119\rightarrow{}^{293}\mathrm{Ts}$	12.40	12.90	−0.0856	−0.073	2	−3.716	−3.561	−4.890	−4.418
$^{298}119\rightarrow{}^{294}\mathrm{Ts}$	12.69	13.09	−0.0806	−0.073	0	−5.037	−5.387	−5.335	−5.430
$^{299}119\rightarrow{}^{295}\mathrm{Ts}$	12.74	13.08	−0.0721	−0.052	2	−4.453	−4.813	−5.218	−5.312
$^{300}119\rightarrow{}^{296}\mathrm{Ts}$	12.55	13.04	−0.0601	−0.032	0	−4.559	−4.939	−5.048	−5.185
$^{301}119\rightarrow{}^{297}\mathrm{Ts}$	12.40	13.08	−0.0494	−0.032	0	−3.977	−4.229	−5.474	−5.483
$^{302}119\rightarrow{}^{298}\mathrm{Ts}$	12.40	13.05	−0.0431	0	0	−4.096	−4.639	−4.925	−5.282
$^{303}119\rightarrow{}^{299}\mathrm{Ts}$	12.39	13.11	−0.0355	0	2	−3.632	−3.256	−5.147	−4.523
$^{304}119\rightarrow{}^{300}\mathrm{Ts}$	12.91	13.86	−0.02	0	0	−4.972	−4.737	−6.519	−6.215
$^{305}119\rightarrow{}^{301}\mathrm{Ts}$	13.40	13.86	0.0147	0	2	−5.650	−5.384	−6.607	−6.250
$^{306}119\rightarrow{}^{302}\mathrm{Ts}$	13.18	13.92	−0.0198	0	0	−5.525	−5.464	−6.631	−6.501
$^{307}119\rightarrow{}^{303}\mathrm{Ts}$	12.76	13.39	−0.0287	0	0	−4.721	−5.152	−6.012	−6.358
$^{308}119\rightarrow{}^{304}\mathrm{Ts}$	12.04	12.17	−0.0396	0.011	0	−3.247	−2.919	−2.970	−2.456
$^{309}119\rightarrow{}^{305}\mathrm{Ts}$	11.35	11.70	−0.0508	0	3	−0.836	−1.338	−1.722	−2.005

Table 6 (continued)

α transition	Q_α^{WS4} (MeV)	Q_α^{FRDM} (MeV)	β_2^{WS4}	β_2^{FRDM}	l	$\log_{10}T_{1/2}^{\mathrm{Cal1}}$	$\log_{10}T_{1/2}^{\mathrm{XGBoost1}}$	$\log_{10}T_{1/2}^{\mathrm{Cal2}}$	$\log_{10}T_{1/2}^{\mathrm{XGBoost2}}$
$^{310}119\rightarrow{}^{306}$Ts	10.86	10.67	−0.0616	−0.032	0	−0.517	−0.651	0.666	0.752
$^{311}119\rightarrow{}^{307}$Ts	10.76	10.32	−0.1895	0	0	0.098	0.171	1.315	1.434
$^{312}119\rightarrow{}^{308}$Ts	10.56	9.90	−0.1936	−0.397	0	−0.908	−0.512	1.916	2.463
$^{313}119\rightarrow{}^{309}$Ts	9.37	10.06	−0.2055	0.066	2	4.825	5.333	2.398	2.812
$^{314}119\rightarrow{}^{310}$Ts	8.97	9.55	−0.2136	−0.407	0	3.896	4.091	3.085	3.233
$^{315}119\rightarrow{}^{311}$Ts	8.65	9.36	−0.2137	−0.406	1	7.318	7.005	4.635	4.535
$^{316}119\rightarrow{}^{312}$Ts	8.67	9.20	−0.2369	−0.406	0	7.050	6.877	5.404	5.308
$^{317}119\rightarrow{}^{313}$Ts	9.20	9.06	−0.4273	−0.416	3	5.859	5.518	6.462	6.180
$^{287}120\rightarrow{}^{283}$Og	13.84	13.96	−0.0531	0.043	4	−5.595	−5.706	−5.729	−5.590
$^{288}120\rightarrow{}^{284}$Og	13.71	13.85	−0.0663	0.064	0	−7.039	−7.317	−7.068	−7.147
$^{289}120\rightarrow{}^{285}$Og	13.69	13.75	−0.0797	0.075	0	−6.253	−6.497	−6.213	−6.227
$^{290}120\rightarrow{}^{286}$Og	13.68	13.75	−0.0872	0.075	0	−7.028	−6.996	−6.852	−6.641
$^{291}120\rightarrow{}^{287}$Og	13.48	13.87	−0.096	0.075	2	−5.586	−6.056	−6.164	−6.394
$^{292}120\rightarrow{}^{288}$Og	13.44	13.78	0.0788	0.086	0	−6.222	−6.226	−6.874	−6.743
$^{293}120\rightarrow{}^{289}$Og	13.37	13.65	0.0786	0.086	2	−5.206	−4.958	−5.741	−5.304
$^{294}120\rightarrow{}^{290}$Og	13.22	13.49	−0.1098	0.086	0	−6.132	−5.759	−6.338	−5.857
$^{295}120\rightarrow{}^{291}$Og	13.25	13.46	0.0762	0.075	2	−4.954	−4.862	−5.386	−5.101
$^{296}120\rightarrow{}^{292}$Og	13.32	13.59	0.0752	0.075	0	−5.989	−6.199	−6.554	−6.624
$^{297}120\rightarrow{}^{293}$Og	13.12	13.65	0.0751	0.075	0	−4.970	−5.153	−6.021	−6.065
$^{298}120\rightarrow{}^{294}$Og	12.98	13.24	−0.0863	0.064	0	−5.595	−5.896	−5.915	−6.019
$^{299}120\rightarrow{}^{295}$Og	13.23	13.73	−0.0849	−0.084	0	−5.343	−5.652	−6.325	−6.379
$^{300}120\rightarrow{}^{296}$Og	13.29	13.70	−0.075	−0.063	0	−6.233	−6.400	−7.155	−7.105
$^{301}120\rightarrow{}^{297}$Og	13.04	13.62	−0.065	−0.042	2	−4.654	−4.944	−5.800	−5.842
$^{302}120\rightarrow{}^{298}$Og	12.87	13.55	0.0382	−0.032	0	−5.155	−5.582	−6.773	−7.067
$^{303}120\rightarrow{}^{299}$Og	12.79	13.51	−0.0448	−0.011	2	−4.104	−3.690	−5.556	−4.860
$^{304}120\rightarrow{}^{300}$Og	12.74	13.55	−0.0355	0	0	−4.999	−5.520	−6.684	−7.019
$^{305}120\rightarrow{}^{301}$Og	13.26	14.26	−0.0214	0	2	−5.060	−4.988	−6.954	−6.729
$^{306}120\rightarrow{}^{302}$Og	13.77	14.28	0.0139	0	0	−6.971	−6.621	−8.042	−7.641
$^{307}120\rightarrow{}^{303}$Og	13.50	13.62	0.0191	0	4	−4.873	−4.879	−5.125	−5.078
$^{308}120\rightarrow{}^{304}$Og	12.95	12.96	−0.0297	0	0	−5.426	−5.655	−5.503	−5.616
$^{309}120\rightarrow{}^{305}$Og	12.14	11.77	−0.0416	−0.021	0	−2.932	−3.279	−2.053	−2.157
$^{310}120\rightarrow{}^{306}$Og	11.48	11.29	−0.0527	0	0	−2.063	−1.779	−1.673	−1.204
$^{311}120\rightarrow{}^{307}$Og	11.18	10.76	−0.1882	−0.397	2	−0.300	−0.385	0.877	1.003
$^{312}120\rightarrow{}^{308}$Og	11.20	10.71	−0.1933	−0.397	0	−1.344	−1.316	−0.251	−0.074
$^{313}120\rightarrow{}^{309}$Og	11.01	10.50	−0.194	−0.407	2	0.160	0.431	1.648	2.098
$^{314}120\rightarrow{}^{310}$Og	10.74	10.33	−0.2019	−0.407	0	−0.043	0.109	0.961	1.208
$^{315}120\rightarrow{}^{311}$Og	9.41	10.16	−0.2323	−0.407	0	4.792	5.516	2.425	2.993
$^{316}120\rightarrow{}^{312}$Og	9.17	9.94	0.3893	−0.416	0	4.035	3.735	2.277	2.114
$^{317}120\rightarrow{}^{313}$Og	9.91	9.83	−0.4157	−0.416	3	3.757	4.187	4.041	4.669
$^{318}120\rightarrow{}^{314}$Og	9.91	9.66	−0.425	−0.416	0	2.772	2.722	3.266	3.408

$\log_{10}T_{1/2}^{\mathrm{XGBoost2}}$) , are in good agreement with the experimental α-decay half-lives. For ^{294}Og, the calculated α-decay half-life obtained by the XGBoost2 model was much closer to the experimental α-decay half-lives than those obtained by other models. Figure 5 reveals that when neutron numbers surpass $N = 184$, the α-decay half-lives of nuclei $Z = 117$, 118, 119, and 120 exhibit a rapid decrease of more than 1.8 orders of magnitude. This phenomenon reflects strong shell effects, suggesting that $N = 184$ is a neutron magic number. Additionally, the decimal logarithms of α-decay half-life values for nuclei with $Z = 117$, 118, 119, and 120 ranged from −8

to 10. If these nuclei could be synthesized in a laboratory, the majority could be detected experimentally.

4 Summary

In summary, this study investigated the impact of deformation effects on α-decay half-lives using an improved formula within the WKB framework. By incorporating the quadrupole deformation of the daughter nucleus into the Coulomb potential, the improved formula provides a refined description of the α-decay half-lives of nuclei with $62 \leqslant Z \leqslant 118$. Although the improved formula does not significantly reduce the overall σ value, it provides calculations that align more closely with the experimental values for nuclei with larger deformations. Furthermore, XGBoost models have been employed to further reduce the deviations between experimental and calculated α-decay half-lives using the improved formula. The results suggest that the XGBoost model can effectively reduce the RMSDs between the calculated and experimental values across all nuclei, including those near magic and sub-magic numbers. Additionally, the improved formula and XGBoost models that yield low σ values were extended to predict α-decay half-lives for nuclei with $Z = 117$, 118, 119, and 120. When neutron numbers surpass $N = 184$, the α-decay half-lives of nuclei $Z = 117$, 118, 119, and 120 exhibit a rapid decrease of more than 1.8 orders of magnitude. These results indicate that $N = 184$ is a magic number.

Author Contributions All authors contributed to the study conception and design. Material preparation, data collection and analysis were performed by Hong-Qiang You, Xiao-Tao He, Ren-Hang Wu, Jing-Jing Li, Qing-Hua He and Hai-Qian Zhang. The first draft of the manuscript was written by Hong-Qiang You, and all authors commented on previous versions of the manuscript. All authors read and approved the final manuscript.

Data availability The data that support the findings of this study are openly available in Science Data Bank at https://cstr.cn/31253.11.sciencedb.25412 and https://doi.org/10.57760/sciencedb.25412.

Declarations

Conflict of interest The authors declare that they have no Conflict of interest.

References

1. R.W. Gurney, E.U. Condon, Wave mechanics and radioactive disintegration. Nature **122**, 1476–4687 (1928). https://doi.org/10.1038/122439a0
2. G. Gamow, Zur quantentheorie des atomkernes. Z. Phys. **51**, 204–212 (1928). https://doi.org/10.1007/BF01343196
3. K. Wei, Y.L. Ye, Z.H. Yang, Clustering in nuclei: progress and perspectives. Nucl. Sci. Tech. **35**, 216 (2024). https://doi.org/10.1007/s41365-024-01588-x
4. M.H. Zhang, Y.H. Zhang, Y. Zou et al., Possibilities for the synthesis of superheavy element $Z = 121$ in fusion reactions. Nucl. Sci. Tech. **35**, 95 (2024). https://doi.org/10.1007/s41365-024-01452-y
5. P.H. Chen, C. Geng, Z.X. Yang et al., Production of neutron-rich actinide isotopes in isobaric collisions via multinucleon transfer reactions. Nucl. Sci. Tech. **34**, 160 (2023). https://doi.org/10.1007/s41365-023-01314-z
6. H. Geiger, J.M. Nuttall, LVII. the ranges of the α particles from various radioactive substances and a relation between range and period of transformation. Philos. Mag. **22**, 613–621 (1911). https://doi.org/10.1080/14786441008637156
7. G. Royer, Alpha emission and spontaneous fission through quasi-molecular shapes. J. Phys. G Nucl. Part. Phys. **26**, 1149–1170 (2000). https://doi.org/10.1088/0954-3899/26/8/305
8. G. Royer, Analytic expressions for alpha-decay half-lives and potential barriers. Nucl. Phys. A **848**, 279–291 (2010). https://doi.org/10.1016/j.nuclphysa.2010.09.009
9. V.E. Viola, G.T. Seaborg, Nuclear systematics of the heavy elements-II lifetimes for alpha, beta and spontaneous fission decay. J. Ino. Nucl. Chem. **28**, 741–761 (1966). https://doi.org/10.1016/0022-1902(66)80412-8
10. D.D. Ni, Z.Z. Ren, T.K. Dong et al., Unified formula of half-lives for α decay and cluster radioactivity. Phys. Rev. C **78**, 044310 (2008). https://doi.org/10.1103/PhysRevC.78.044310
11. Y.J. Ren, Z.Z. Ren, New geiger-nuttall law for α decay of heavy nuclei. Phys. Rev. C **85**, 044608 (2012). https://doi.org/10.1103/PhysRevC.85.044608
12. C. Qi, F.R. Xu, R.J. Liotta et al., Universal decay law in charged-particle emission and exotic cluster radioactivity. Phys. Rev. Lett. **103**, 072501 (2009). https://doi.org/10.1103/PhysRevLett.103.072501
13. J.G. Deng, H.F. Zhang, G. Royer, Improved empirical formula for α-decay half-lives. Phys. Rev. C **101**, 034307 (2020). https://doi.org/10.1103/PhysRevC.101.034307
14. V.Y. Denisov, A.A. Khudenko, α-decay half-lives: empirical relations. Phys. Rev. C **79**, 054614 (2009). https://doi.org/10.1103/PhysRevC.79.054614
15. D.N. Poenaru, D.T. Akrawy, Alpha decay calculations with a new formula. J. Phys. G: Nucl. Part. Phys. **44**, 105105 (2017). https://doi.org/10.1088/1361-6471/aa8527
16. D.T. Akrawy, A.H. Ahmed, New empirical formula for α-decay calculations. Int. J. Mod. Phys. E **27**, 1850068 (2018). https://doi.org/10.1142/s0218301318500684
17. E. Shin, Y. Lim, C.H. Hyun et al., Nuclear isospin asymmetry in α decay of heavy nuclei. Phys. Rev. C **94**, 024320 (2016). https://doi.org/10.1103/PhysRevC.94.024320
18. J.M. Dong, H.F. Zhang, Y.Z. Wang et al., Alpha-decay for heavy nuclei in the ground and isomeric states. Nucl. Phys. A **832**, 198–208 (2010). https://doi.org/10.1016/j.nuclphysa.2009.10.082
19. Z.Y. Wang, Z.M. Niu, Q. Liu et al., Systematic calculations of α -decay half-lives with an improved empirical formula. J. Phys. G Nucl. Part. Phys. **42**, 055112 (2015). https://doi.org/10.1088/0954-3899/42/5/055112
20. D.T. Akrawy, H. Hassanabadi, Y. Qian et al., Influence of nuclear isospin and angular momentum on α-decay half-lives. Nucl. Phys. A **983**, 310–320 (2019). https://doi.org/10.1016/j.nuclphysa.2018.10.091
21. D.T. Akrawy, A.H. Ahmed, α-decay systematics for superheavy nuclei. Phys. Rev. C **100**, 044618 (2019). https://doi.org/10.1103/PhysRevC.100.044618
22. Y.B. Qian, Z.Z. Ren, Unfavored α decay from ground state to ground state in the range $53 \leq Z \leq 91$. Phys. Rev. C **85**, 027306 (2012). https://doi.org/10.1103/PhysRevC.85.027306

23. S.Q. Guo, X.J. Bao, Y. Gao et al., The nuclear deformation and the preformation factor in the α-decay of heavy and superheavy nuclei. Nucl. Phys. A **934**, 110–120 (2015). https://doi.org/10.1016/j.nuclphysa.2014.12.001
24. K.M.K. Sharma, Cluster radioactivity within the collective fragmentation approach using different mass tables and related deformations. Eur. Phys. J. A **56**, 35 (2020). https://doi.org/10.1140/epja/s10050-020-00023-0
25. Y.B. Qian, Z.Z. Ren, D.D. Ni, Calculations of α-decay half-lives for heavy and superheavy nuclei. Phys. Rev. C **83**, 044317 (2011). https://doi.org/10.1103/PhysRevC.83.044317
26. C. Xu, Z.Z. Ren, Global calculation of alpha-decay half-lives with a deformed density-dependent cluster model. Phys. Rev. C **74**, 014304 (2006). https://doi.org/10.1103/PhysRevC.74.014304
27. W. Seif, A. Adel, N. Antonenko et al., Enhanced α decays to negative-parity states in even-even nuclei with octupole deformation. Phys. Rev. C **107**, 044601 (2023). https://doi.org/10.1103/PhysRevC.107.044601
28. W. Yahya, O. Azeez, J. Majekodunmi et al., Density-dependent parametrizations in B3Y-Fetal NN interaction: application to alpha decay. Int. J. Theo. Phys **54**, 74 (2024). https://doi.org/10.1007/s13538-024-01453-7
29. H.F. Gui, X.J. Liu, H. Mand Wu, P.C. Chu et al., Systematic study of α decay half-lives for even-even nuclei within a deformed two-potential approach. Commun. Theor. Phys. **74**, 055301 (2022). https://doi.org/10.1088/1572-9494/ac6576
30. Y. Xin, N.N. Ma, J.G. Deng et al., Properties of $Z = 114$ superheavy nuclei. Nucl. Sci. Tech. **32**, 55 (2021). https://doi.org/10.1007/s41365-021-00899-7
31. S.H. Cheng, Z.S. Ge, L.G. Cao et al., Theoretical calculations of the nuclear deformation effects on α-decay half-lives for heavy and super-heavy nuclei. J. Phys. G **48**, 095106 (2021). https://doi.org/10.1088/1361-6471/ac165f
32. D. Naderi, M. Zargooshi, Study of alpha-decay half-lives with deformed, oriented daughter nuclei. Int. J. Mod. Phys. E **24**, 1550010 (2015). https://doi.org/10.1142/S021830131550010X
33. M. Pahlavani, S. Alavi, N. Tahanipour, Effect of nuclear deformation on the potential barrier and alpha-decay half-lives of superheavy nuclei. Mod. Phys. Lett. A **28**, 1350065 (2013). https://doi.org/10.1142/S021773231350065X
34. A. Boehnlein, M. Diefenthaler, N. Sato et al., Colloquium: machine learning in nuclear physics. Rev. Mod. Phys. **94**, 031003 (2022). https://doi.org/10.1103/RevModPhys.94.031003
35. W.B. He, Q.F. Li, Y.G. Ma et al., Machine learning in nuclear physics at low and intermediate energies. Sci. China. Phys. Mech. **66**, 282001 (2023). https://doi.org/10.1007/s11433-023-2116-0
36. B.S. Cai, C. Yuan, Random forest-based prediction of decay modes and half-lives of superheavy nuclei. Nucl. Sci. Tech. **34**, 204 (2023). https://doi.org/10.1007/s41365-023-01354-5
37. S. Akkoyun, T. Bayram, S.O. Kara et al., An artificial neural network application on nuclear charge radii. J. Phys. G Nucl. Part. Phys. **40**, 055106 (2013). https://doi.org/10.1088/0954-3899/40/5/055106
38. T. Bayram, S. Akkoyun, S.O. Kara, A study on ground-state energies of nuclei by using neural networks. Ann. Nucl. Energy **63**, 172–175 (2014). https://doi.org/10.1016/j.anucene.2013.07.039
39. W.C. Chen, R. Utama, J. Piekarewicz, Nuclear charge radii: density functional theory meets Bayesian neural networks. J. Phys. G **43**, 114002 (2016). https://doi.org/10.1088/0954-3899/43/11/114002
40. L. Neufcourt, Y. Cao, W. Nazarewicz et al., Bayesian approach to model-based extrapolation of nuclear observables. Phys. Rev. C **98**, 034318 (2018). https://doi.org/10.1103/PhysRevC.98.034318
41. Z.M. Niu, H.Z. Liang, Nuclear mass predictions based on Bayesian neural network approach with pairing and shell effects. Phys. Lett. B **778**, 48–53 (2018). https://doi.org/10.1016/j.physletb.2018.01.002
42. Z.M. Niu, H.Z. Liang, B.H. Sun et al., Predictions of nuclear β -decay half-lives with machine learning and their impact on r -process nucleosynthesis. Phys. Rev. C **99**, 064307 (2019). https://doi.org/10.1103/PhysRevC.99.064307
43. G. Saxena, P.K. Sharma, P. Saxena, Modified empirical formulas and machine learning for α-decay systematics. J. Phys. G Nucl. Part. Phys. **48**, 055103 (2021). https://doi.org/10.1088/1361-6471/abcd1c
44. Z.M. Niu, H.Z. Liang, Nuclear mass predictions with machine learning reaching the accuracy required by r-process studies. Phys. Rev. C **106**, L021303 (2022). https://doi.org/10.1103/PhysRevC.106.L021303
45. H.Q. You, Z.Z. Qu, R.H. Wu et al., Study on nuclear α-decay energy by an artificial neural network with pairing and shell effects. Symmetry **5**, 1006 (2022). https://doi.org/10.3390/sym14051006
46. C.Q. Li, C.N. Tong, H.J. Du et al., Deep learning approach to nuclear masses and α-decay half-lives. Phys. Rev. C **105**, 064306 (2022). https://doi.org/10.1103/PhysRevC.105.064306
47. A.E. Lovell, A.T. Mohan, T.M. Sprouse et al., Nuclear masses learned from a probabilistic neural network. Phys. Rev. C **106**, 014305 (2022). https://doi.org/10.1103/PhysRevC.106.014305
48. X.X. Dong, R. An, J.X. Lu et al., Novel Bayesian neural network based approach for nuclear charge radii. Phys. Rev. C **105**, 014308 (2022). https://doi.org/10.1103/PhysRevC.105.014308
49. Z. Yuan, D. Bai, Z. Wang et al., Reliable calculations of nuclear binding energies by the gaussian process of machine learning. Nucl. Sci. Tech. **35**, 105 (2024). https://doi.org/10.1007/s41365-024-01463-9
50. Q.F. Song, L. Zhu, J. Su, Target dependence of isotopic cross sections in the spallation reactions ^{238}U + p and ^{9}Be at 1 AGeV *. Chin. Phys. C **46**, 074108 (2022). https://doi.org/10.1088/1674-1137/ac6249
51. T.X. Huang, X.H. Wu, P.W. Zhao, Application of kernel ridge regression in predicting neutron-capture reaction cross-sections. Commun. Theor. Phys. **74**, 095302 (2022). https://doi.org/10.1088/1572-9494/ac763b
52. F. Li, Y. Wang, Z. Gao et al., Application of machine learning in the determination of impact parameter in the ^{132}Sn +^{124} Sn system. Phys. Rev. C **104**, 034608 (2021). https://doi.org/10.1103/PhysRevC.104.034608
53. X. Zhang, X. Liu, Y. Huang et al., Determining impact parameters of heavy-ion collisions at low-intermediate incident energies using deep learning with convolutional neural networks. Phys. Rev. C **105**, 034611 (2022). https://doi.org/10.1103/PhysRevC.105.034611
54. L. Yang, C.J. Lin, Y.X. Zhang et al., Bayesian analysis on interactions of exotic nuclear systems. Phys. Lett. B **807**, 135540 (2020). https://doi.org/10.1016/j.physletb.2020.135540
55. Y.D. Song, R. Wang, Y.G. Ma et al., Determining the temperature in heavy-ion collisions with multiplicity distribution. Phys. Lett. B **814**, 136084 (2021). https://doi.org/10.1016/j.physletb.2021.136084
56. M. Omana Kuttan, J. Steinheimer, K. Zhou et al., The QCD EoS of dense nuclear matter from Bayesian analysis of heavy ion collision data. (2022). arXiv:2211.11670, https://doi.org/10.48550/arXiv.2211.11670
57. W.J. Xie, B.A. Li, Bayesian inference of the symmetry energy of superdense neutron-rich matter from future radius measurements of massive neutron stars. Astrophys. J **899**, 4 (2020). https://doi.org/10.3847/1538-4357/aba271
58. S.L. Chen, T.X. Wang, Z. Zhang et al., Linear regression and machine learning for nuclear forensics of spent fuel from six types

of nuclear reactors. Phys. Rev. Appl. **19**, 034028 (2023). https://doi.org/10.1103/PhysRevApplied.19.034028
59. T. Li, Y. Chen, S.B. Wang et al., Reconstruction of the event vertex in the PandaX-III experiment with convolution neural network. J. High. Engergy. Phys. **2023**, 200 (2023). https://doi.org/10.1007/JHEP05(2023)200
60. V.Y. Denisov, A. Khudenko, α-decay half-lives, α-capture, and α-nucleus potential. At. Data Nucl. Data Tables **95**, 815–835 (2009). https://doi.org/10.1016/j.adt.2009.06.003
61. M. Ismail, A. Ellithi, M. Botros et al., Penetration factor in deformed potentials: application to α decay with deformed nuclei. Phys. Rev. C **86**, 044317 (2012). https://doi.org/10.1103/PhysRevC.86.044317
62. R.K. Gupta, A. Săndulescu, W. Greiner, Interaction barriers, nuclear shapes and the optimum choice of a compound nucleus reaction for producing super-heavy elements. Phys. Lett. B **67**, 257–261 (1977). https://doi.org/10.1016/0370-2693(77)90364-1
63. N. Malhotra, R.K. Gupta, Proximity potential for deformed, oriented collisions and its application to ^{238} U + ^{238} U. Phys. Rev. C **31**, 1179 (1985). https://doi.org/10.1103/PhysRevC.31.1179
64. T. Chen, C. Guestrin, in *Proceedings of the 22nd ACM SIGKDD International Conference on Knowledge Discovery and Data Mining*, Xgboost: a scalable tree boosting system. KDD '16, (Association for Computing Machinery, New York, NY, USA, 2016), pp. 785–794. https://doi.org/10.1145/2939672.2939785
65. F. Kondev, M. Wang, W. Huang et al., The NUBASE2020 evaluation of nuclear physics properties *. Chin. Phys. C **45**, 030001 (2021). https://doi.org/10.1088/1674-1137/abddae
66. M. Wang, W. Huang, F. Kondev et al., The AME 2020 atomic mass evaluation (ii). tables, graphs and references*. Chin. Phys. C **45**, 030003 (2021). https://doi.org/10.1088/1674-1137/abddaf
67. N. Wang, M. Liu, X. Wu et al., Surface diffuseness correction in global mass formula. Phys. Lett. B **734**, 215–219 (2014). https://doi.org/10.1016/j.physletb.2014.05.049
68. P. Möller, A. Sierk, T. Ichikawa et al., Nuclear ground-state masses and deformations: Frdm (2012). At. Data Nucl. Data Tables **109–110**, 1–204 (2016). https://doi.org/10.1006/adnd.1995.1002
69. X.J. Bao, H.F. Zhang, G. Royer et al., Spontaneous fission half-lives of heavy and superheavy nuclei within a generalized liquid drop model. Nucl. Phys. A **906**, 1–13 (2013). https://doi.org/10.1016/j.nuclphysa.2013.03.002
70. G. Lalazissis, M. Sharma, P. Ring et al., Superheavy nuclei in the relativistic mean-field theory. Nucl. Phys. A **608**, 202–226 (1996). https://doi.org/10.1016/0375-9474(96)00273-4
71. R. Smolańczuk, J. Skalski, A. Sobiczewski, Spontaneous-fission half-lives of deformed superheavy nuclei. Phys. Rev. C **52**, 1871–1880 (1995). https://doi.org/10.1103/PhysRevC.52.1871
72. https://t2.lanl.gov/nis/data/astro/molnix96/spidat.html